Materials Today Catalysis 9 (2025) 100100

Contents lists available at ScienceDirect

Materials Today Catalysis

journal homepage: www.journals.elsevier.com/materials-today-catalysis

Investigating size-dependent selectivity in benzaldehyde reductive amination via Ni nanoparticles

Yunong Li [a,b], Ching Kit Tommy Wun [a,b], Tianxiang Chen [a,b,*], Tsz Woon Benedict Lo [a,b,c,*]

[a] State Key Laboratory of Chemical Biology and Drug Discovery, Department of Applied Biology and Chemical Technology, The Hong Kong Polytechnic University, Hung Hom, Hong Kong SAR
[b] The Hong Kong Polytechnic University Shenzhen Research Institute, The Hong Kong Polytechnic University, Shenzhen 518057, China
[c] Department of Applied Physics, The Hong Kong Polytechnic University, Hung Hom, Hong Kong SAR

ARTICLE INFO

Keywords:
Ni nanoparticle
Size effect
Reductive amination reaction
Precise control
In-situ characterization
Catalyst design

ABSTRACT

Selectivity control is a fundamental focus in catalysis chemistry, as it directly reflects the efficiency and efficacy of catalytic processes. While catalysis often involves intricate and cascade reaction steps using nanoparticle (NP) catalysts, the mechanism behind the size effect of nanoparticles on product selectivity has not been fully explored. We herein prepared a series of Ni-containing zeolitic catalysts in which the Ni NPs are uniformly supported on the mesopores and outer surfaces of H-ZSM-5 zeolites. The dynamic formation of Ni NPs from highly dispersed Ni precursors was monitored using transmission electron microscopy, in-situ X-ray pair distribution function, and in-situ X-ray absorption fine structure analysis. The metal nanoparticle size was carefully controlled between 3.72(5) nm and 11.91(7) by controlling the reduction temperature. We evaluated the catalytic performance of Ni NPs using the reductive amination of benzaldehyde in batch reactors at low temperatures. This reaction inherently favors the formation of a series of products, suffering highly from selectivity issues. Our results revealed a size-dependent behavior in reaction efficiency, with the catalyst achieving the highest catalytic activity (93 % selectivity in primary amine) at a particle size of 5.62(3) nm. This optimal performance is attributed to a balanced interplay between hydrogenation and amination capabilities. These findings highlight the intricate relationship between nanoparticle size and catalytic performance, emphasizing the necessity for precise optimization in catalyst design to enhance selectivity and sustainability in industrial applications.

1. Introduction

The sustainable supply of chemical products is a major policy concern in numerous countries [1]. In the realm of sustainable production, heterogeneous catalysts are extensively used and hold great promise, attributed to their remarkable chemical stability and recyclability [2,3]. In heterogeneous catalytic processes, aside from the catalyst cost and lifetime, reactivity and selectivity are typically the most crucial factors to be considered. In most reaction processes, the reactivity can be enhanced by simply raising the reaction temperature. Nevertheless, these catalytic processes suffer significantly from selectivity issues as the reaction temperature rises. Decreased selectivity may result in several problems, such as more waste, elevated purification costs, and heightened environmental concerns [4]. Prominent examples are the hydrogenation of alkynes and the reductive amination of carbonyls for the production of primary, secondary, and tertiary amines [5–9].

The process of reductive amination of carbonyls entails the formation of intermediate imine/iminium species from ammonia sources succeeded by reduction [10,11]. Common selectivity issues encompass overalkylation [12], chemo-selectivity [9], regioselectivity [13], and competing side reactions [14]. To enhance efficiency and sustainability in commercial synthesis, it is crucial to meticulously optimize the reduction agent and reaction conditions, as well as emphasize the hydrogenation and amination capabilities. In addition to the noble-metal-based catalysts [15,16], various metal-loaded catalysts have been explored for this reaction. Among them, Ni-based catalysts,

* Corresponding authors at: State Key Laboratory of Chemical Biology and Drug Discovery, Department of Applied Biology and Chemical Technology, The Hong Kong Polytechnic University, Hung Hom, Hong Kong SAR.
E-mail addresses: yunong.li@connect.polyu.hk (Y. Li), tommy.wun@connect.polyu.hk (C.K.T. Wun), selwin.tx.chen@polyu.edu.hk (T. Chen), twblo@polyu.edu.hk (T.W.B. Lo).

https://doi.org/10.1016/j.mtcata.2025.100100
Received 12 February 2025; Received in revised form 15 April 2025; Accepted 28 April 2025
Available online 29 April 2025

such as Raney Ni, are widely used for selective hydrogenation [17,18]. However, these catalysts require precise calibration to prevent over-reduction. It is well-known that the catalyst size affects certain key structural descriptors of the catalyst at the molecular level, such as the active surface area and the adsorption behavior of key reaction substrates [19,20]. The hydrogenation and amination capacity of catalysts vary with the size of nanoparticles.[21,22] However, the mechanism by which these differences influence the reaction selectivity of the final products remains a challenge.

In this study, we present a comprehensive exploration of the impact of Ni nanoparticle size on the reductive amination of benzaldehyde, especially on product distributions. We meticulously examined the physicochemical and structural attributes of a series of ZSM-5 zeolite-supported Ni nanoparticles (NPs) with precisely controlled sizes ranging from 3.72(5) nm to 11.91(7) nm. Our investigation incorporated a range of characterization methodologies, including transmission electron microscopy (TEM), X-ray pair distribution function (PDF) analysis, and X-ray absorption fine structure (XAFS) analysis. To evaluate the catalytic performance, we conducted experiments in batch reactors at 70 °C and 90 °C. Among the catalysts analyzed, the Ni/Z[5.62] sample exhibited the highest catalytic activity with a selectivity of 93.0 %. Our mechanism study further unveiled a size-dependent behavior in the reductive amination of benzaldehyde over the supported Ni NPs, in which the Ni/Z[5.62] demonstrated an optimal balance between its hydrogenation and amination abilities.

2. Experimental section

The procedures for the preparation, characterization techniques, model reaction methods, and structure refinement parameters of the catalysts are detailed in the supporting materials.

3. Results and discussion

3.1. Characterization of the structure of Ni/Z[D] catalysts

A H-ZSM-5 zeolite with a SiO_2:Al_2O_3 ratio of 46 was selected as the host in this study. This zeolite was chosen for its exceptional crystallinity and uniform distribution of Brønsted acid sites, enabling the loading of a controlled concentration of Ni through ion exchange with Ni(II) bis (acetylacetonate) ($Ni(acac)_2$). Detailed characterization of the physicochemical properties of the H-ZSM-5 zeolite is provided in Figure S1 and Table S1 of the Supporting Information (SI). As shown in our previous work, this ZSM-5 zeolite possesses a meso-microporous hierarchical structure, with a micropore size of around 5 Å and a mesopore size between 20 Å – 50 Å [23]. The Ni content was quantified as 3.0 wt% using ICP-OES (Table S2). Transmission electron microscopy (TEM, Fig. 1**a–g**) and energy dispersive X-ray spectroscopy (EDX) analysis were made to confirm the absence of metal aggregation in the Ni-containing zeolitic samples (referred to as 'Ni-Z'), demonstrating the effectiveness of the Ni incorporation process. Furthermore, no Bragg peaks in powder X-ray diffraction (XRD, Figure S2) can be ascribed to the crystalline Ni species, indicating the absence of Ni aggregation in the precursors.

To prepare Ni NPs of varying sizes, controlled reduction under hydrogen at different reaction temperatures was employed. Initially, a series of TEM measurements were conducted to assess the sizes of the Ni NPs, as illustrated in Fig. 1. EDX analyses showcased a uniform and highly dispersed distribution of Ni both before and after reduction (denoted as 'Ni/Z[D]', where D represents the nanoparticle diameter in nm). In the TEM images of the Ni/Z[D] samples (as shown in Fig. 1**b–g**), a noticeable enlargement of the Ni NPs is observed with increasing reduction temperatures, with the Ni NPs becoming discernible starting from Ni/Z[3.72]. It is observed that at reduction temperatures below 300 °C, the Ni(II) species has not been sufficiently reduced to form larger nanoparticles, a phenomenon in line with our TEM measurements and previous literature [20,24,25]. This behavior aligns with the typical reduction patterns of isolated Ni species within zeolites during the onset

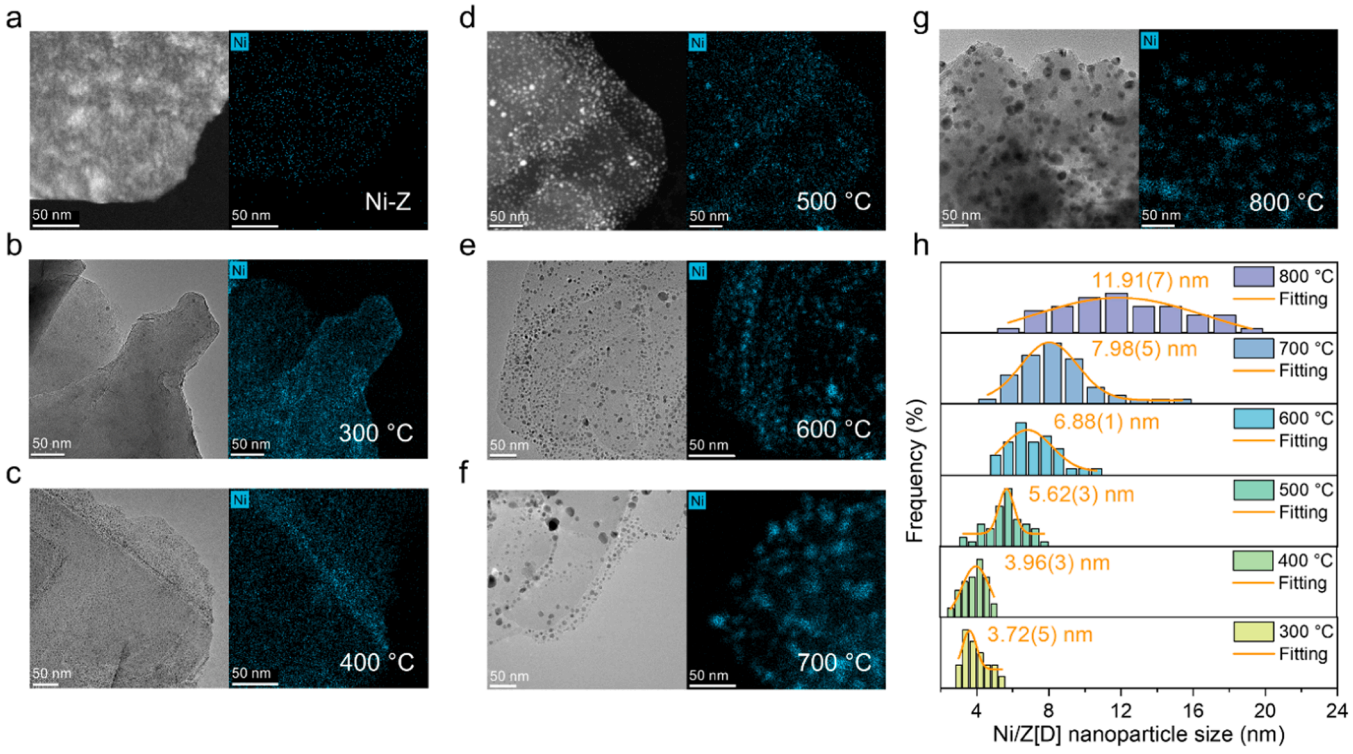

Fig. 1. Morphology characterization of Ni/[D] catalysts reduced at different temperatures. TEM images and EDS mapping of (a) Ni-Z, (b) Ni/Z[3.72], (c) Ni/Z[3.96], (d) Ni/Z[5.62], (e) Ni/Z[6.88], (f) Ni/Z[7.98], (g) Ni/Z[11.91]. (h) The size distribution of Ni NPs obtained from TEM images.

of chemical reduction. The frequency distributions of nanoparticle sizes are depicted in Fig. 1**h**, ranging from 3.72(5) nm at a reduction temperature of 300 °C to 11.91(7) nm at 800 °C. The size of 3.72(5) nm notably exceeds the largest free-sphere dimension of ZSM-5 zeolite (approximately 0.64 nm at the microporous framework intersection), suggesting that the Ni NPs should migrate out of the micropores once the Ni species are reduced and formed particles. In addition, X-ray photoelectron spectroscopy (XPS) analyses were conducted to assess the chemical state of Ni within the catalyst. These measurements revealed a progressive evolution of NiO or Ni^{2+} anchored by BASs to metallic Ni with increasing reduction temperatures (Figure S3 and Table S3).

Building upon the insightful findings from the nanoparticle size analysis, in-situ synchrotron measurements under a reduction environment were employed to investigate the bulk structural properties and understand the structural reorganization during Ni NPs formation.

In-situ synchrotron XRD analysis under a reduction environment (with an energy of 23.229 keV and a wavelength of 0.53375 Å) provided insights into lattice volume trends and metal migration dynamics. Through the measurements, ZSM-5 support was found to maintain high crystallinity even at elevated temperatures (Figure S4). By employing Pawley refinement through TOPAS v7.0 software on the XRD data (Figure S5 and Table S4), it was established that the Ni/Z[D] catalyst retained an orthorhombic crystal system without any phase change. Further analysis revealed a noticeable decrease in lattice volume with rising temperatures, commencing at 5400 $Å^3$ (Fig. 2**a**). This reduction signifies the migration of metal species from micropores to mesopores or external surfaces, which may caused by the distinct topological structure of ZSM-5 zeolite. ZSM-5 contains a zigzag channel (5.1 Å × 5.5 Å) along the a-axis and a straight channel (5.3 Å × 5.6 Å) along the b-axis[26]. Remarkable modifications in the lattice parameters of Ni-Z, particularly along the b-axis, were observed during the reduction process. The b-axis underwent expansion followed by contraction within the temperature range of 300 °C to 800 °C. This behavior can be attributed to the straight channels along the b-axis, which offer lower diffusion resistance[27].

Consequently, the metal tends to preferentially migrate towards the b-axis channels and aggregate. This phenomenon results in a decrease in lattice parameters along the a- and c-axis and an increase along the b-axis. As the metal particles aggregate beyond the pore capacity and are released from the pores, it causes a reduction in the parameter along the b-axis. This dynamic lattice evolution highlights metal aggregation within the zeolite support.

Subsequently, in-situ synchrotron PDF analysis under reduction environment (with an energy of 59.999 keV and a wavelength of 0.20664 Å) was employed to investigate the dynamic structural changes in Ni-Z. In Fig. 2**b**, notable alterations in the distribution of Ni-Ni and Ni-O pairs are observed during reduction. The decline in Ni-O pairs (3.09 Å) is accompanied by the enhancement of Ni-Ni pairs (2.45 Å and 4.23 Å), particularly evident above 527 °C. Notably, at extended distances (4.36 Å and 6.66 Å), the increased peak area of Ni-Ni pairs indicated the aggregation of Ni NPs into larger sizes. These findings are further supported by the differential PDF (dPDF) data in Fig. 2**c**. The progression of the oscillation period from 6.81 Å (27 °C) to 86.36 Å (777 °C) during reduction signifies the enlargement of Ni NPs.

Expanding on the findings from the nanoparticle size analysis and the subsequent X-ray scattering measurements, which show the structural evolution during Ni nanoparticle formation, additional in-situ reduction XAS measurements were carried out to unveil the evolving structural characteristics of the samples throughout the preparation process. Fig. 3**a** shows the XAS data at the Ni K-edge of Ni-Z undergoing hydrogen reduction from 70 °C to 600 °C. The X-ray absorption near edge structure (XANES) of Ni-Z exhibits a reduction from Ni(II) to metallic Ni(0). The most prominent transition occurs around 300 °C, aligning with the structural characterization results discussed earlier.

The in-situ extended X-ray absorption fine structure (EXAFS) datasets in the R-space, as depicted in Fig. 3**b**, reveal intriguing insights into the structural changes occurring during the temperature-induced evolution of the samples. At temperatures below 250 °C, two distinct peaks are noticeable at radial distances (R) of approximately 1.53 Å and 2.64 Å, corresponding to the backscattering of the Ni-O path. As the temperature increases, the intensity of these peaks rapidly decreases within the temperature range of 250 °C to 300 °C. Starting from around 300 °C, the peak at ~ 2.1 Å undergoes a sharp increase, indicating the

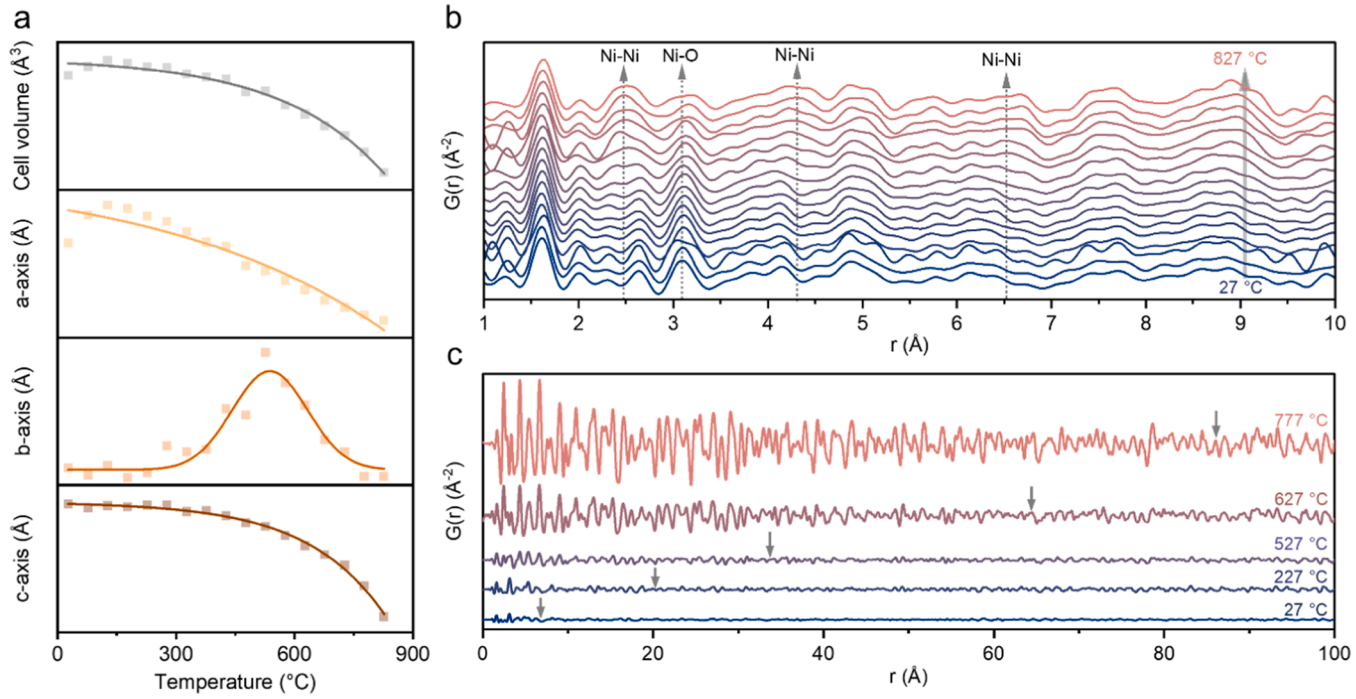

Fig. 2. Structural evolution of Ni-Z catalyst obtained through in-situ synchrotron measurements under reduction environment, tracking from room temperature to 827 °C. (a) Cell volume and lattice parameters obtained through Pawley refinement of XRD measurements (E = 23.229 keV, λ = 0.53375 Å). (b) PDF patterns ranging from 1.0 Å to 10.0 Å (E = 59.999 keV, λ = 0.20664 Å). (c) Differential PDF patterns ranging from 0.0 Å to 100.0 Å.

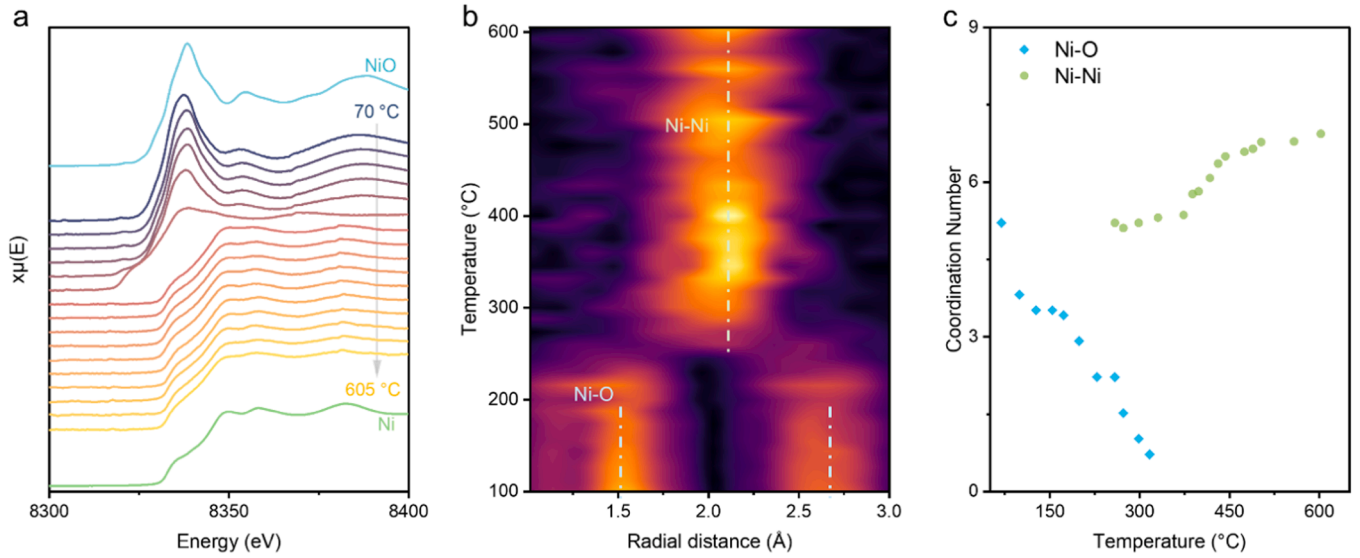

Fig. 3. Structural evolution of loading Ni NPs obtained through synchrotron in-situ reduction XAS, tracking from room temperature to 605 °C. (a) In-situ reduction XAS measurements capturing data at the Ni K-edge. (b) Contour plot depicting R-space in the EXAFS data ranging from 1.0 Å to 3.0 Å. (c) Quantitative evaluation of coordination numbers for Ni-O and Ni-Ni interaction.

emergence of backscattering contributions from the Ni-Ni path. The shift of paths hints at the evolving structural configuration, signifying the formation of Ni NPs during reduction.

The quantitative fitting analysis of the extended X-ray absorption fine structure (EXAFS) datasets (Figure S6 and Table S5) has provided crucial insights into the coordination environment of Ni NPs, as illustrated in Fig. 3**c**. The analysis reveals a decrease in the coordination number (CN) of the Ni-O path from 5.2 (at 70 °C) to 0.8 (at 332 °C), alongside an increase in the CN of the Ni-Ni path from 5.2 (at 300 °C) to 6.9 (at 605 °C). This shift in CN directly shows the aggregation process of Ni. This result aligns with the trend of increasing Ni particle sizes unveiled by TEM measurements. For an in-depth discussion on the relationship between coordination number and nanoparticle size, readers can refer to a book chapter authored by our group [28]. It is noteworthy that during the rapid decrease in Ni-O CN from 250 °C to 350 °C, the Ni-Ni CN remains relatively constant at around 5. This phenomenon could be attributed to the confinement effect exerted by the microporous structure of the zeolite support, influencing the coordination dynamics within the system.

3.2. Catalytic performance and reaction mechanism

Considering the intricate interplay among catalyst structure, nanoparticle size, and catalytic behavior, it becomes essential to integrate the findings from structural analyses with subsequent catalytic assessments. Following a thorough characterization of the Ni/Z[D] catalysts, the reductive amination of benzaldehyde was employed as a model reaction to evaluate catalytic performance. This correlation offers a holistic perspective on how the structural attributes of the Ni NPs influence the catalytic effect in the reductive amination of benzaldehyde.

The comprehensive analysis of multiple measurements revealed that the samples exhibited metallic Ni-Ni characteristics only at reduction temperatures surpassing 300 °C [20]. Consequently, catalytic properties were evaluated exclusively by using samples prepared within the reduction temperature range of 300 °C to 800 °C. As depicted in Scheme 1, the reductive amination reaction possesses a range of amination and hydrogenation products (**2a–2e**) from the initial benzaldehyde substrate (**1**), where benzylamine (**2a**) is commonly recognized as the target product. The comparison of the product selectivity would provide valuable insights into the catalytic efficacy of the samples.

Fig. 4 illustrates the product distribution from the reductive amination of benzaldehyde over Ni/Z[D] at reaction temperatures of 70 °C (**a**) and 90 °C (**b**) (refer to experimental details in the SI). The primary focus is on the catalysis dataset collected at 70 °C as it provides dynamic insights for comprehending the structure-activity relationships. A distinctive volcano trend is observed for product **2a**, with Ni/Z[5.62] exhibiting the highest **2a** selectivity of 93 %. In contrast, Ni/Z[11.91] does not produce any **2a** product but selects a significant portion of product **2b** (the precursor of **2a** before the hydrogenation step). As depicted in Scheme 2, benzaldehyde (**1**) initially reacts with ammonia to generate the amino(phenyl)methanol intermediate, which is subsequently dehydrated to form an imine intermediate before undergoing hydrogenation to produce the target product **2a** [29,30]. The hydrogenation capability of the catalyst plays a crucial role in the hydrogenation

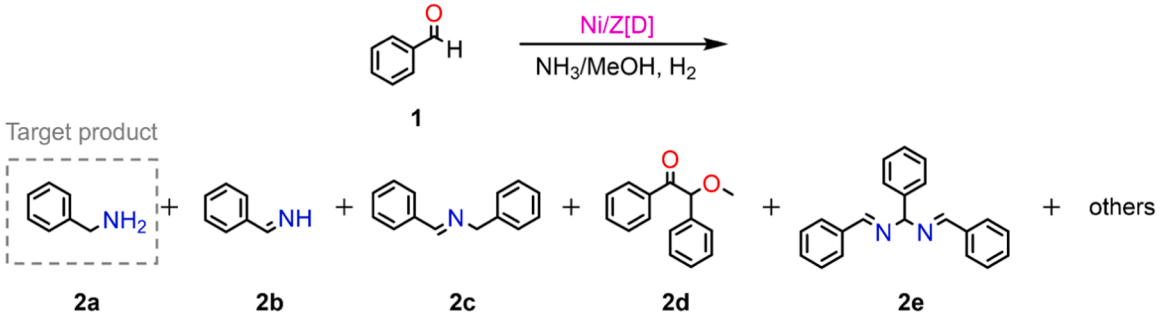

Scheme 1. Reductive amination of benzaldehyde.

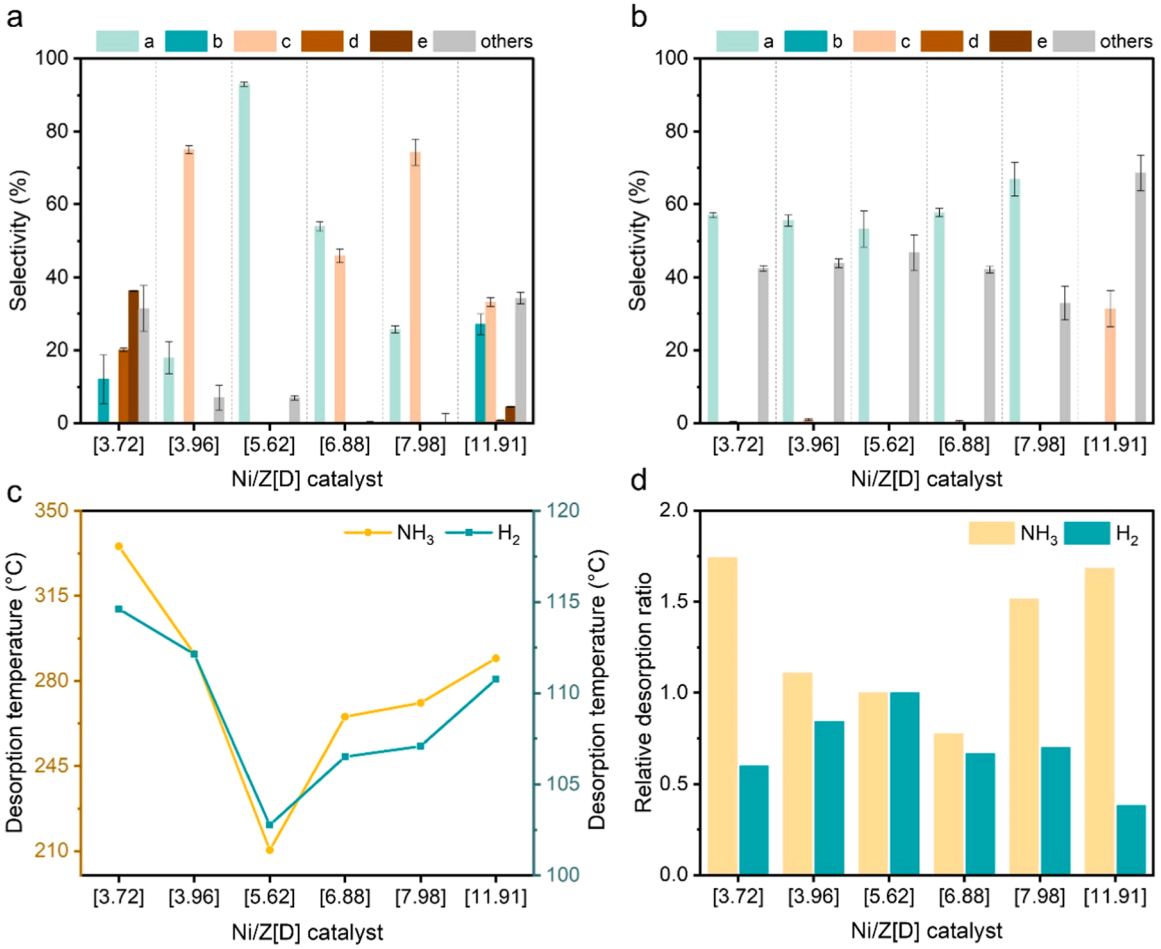

Fig. 4. Catalytic results and surface analyses of Ni/Z[D] catalysts in reductive amination of benzaldehyde. (a) Data collected at 70 °C. (b) Data collected at 90 °C. (c) NH_3-TPD and H_2-TPD analyses of (c) desorption temperatures and (d) the relative ratio of integral adsorption quantities.

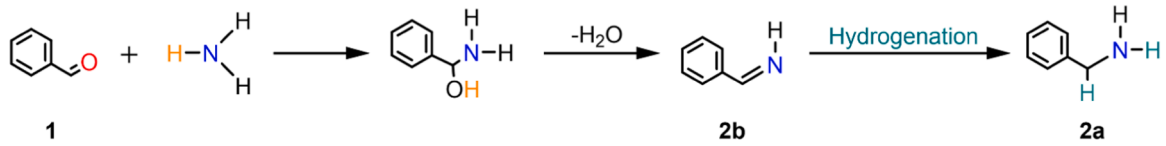

Scheme 2. Main reaction pathway in the reductive amination of benzaldehyde.

of **2b** to **2a**. Adequate surface hydrogen species must be available to ensure efficient hydrogenation of **2b**. The performance of Ni/Z[11.91] can be attributed to a lower hydrogen coverage compared to other Ni/Z[D] samples, as observed in the TPD experiments (Figs. 4**c** and 4**d**).

In addition, a series of by-products, such as **2c**, **2d**, and **2e**, are observed. These by-products originate from a series of competitive reactions, as summarized in Scheme 3. Product **2c** originates from the addition of imine (**2b**) to primary amine (**2a**). The stronger adsorption capacity of imine on the Ni surface compared to the substrate impacts the surface substrate concentration. Concurrently, inadequate hydrogen surface coverage hinders imine conversion to primary amine, promoting competitive reaction (I) and augmenting the formation of **2c** [29]. Moreover, **2d** is selected from a series of tandem reactions involving the reactant and methanol solvent, indicating weak hydrogenation amination capabilities, while **2e** can be attributed to over-amination (*cf.* competitive reactions (II) [31] & (III) [32] in Scheme 3). The interconversion of these products demonstrates a delicate balance among the catalytic capabilities in hydrogenation, amination, and the interactions between substrates and intermediate products.

To further explore the impact of Ni NPs size on the hydrogenation and amination capacity of the catalysts, the reaction temperature was increased to 90 °C. In the catalytic performance at 90 °C (Fig. 4**b**), it can observe highly comparable selectivity at around 60 % of target **2a** over Ni/Z[3.72], Ni/Z[3.96], Ni/Z[5.62], Ni/Z[6.88] and Ni/Z[7.98]. The rise in reaction temperature substantially reduces the difference in product selectivity, with the majority of by-products being polyaromatics (with -Ph > 3). This aligns with existing literature, which indicates that a substantial amount of polyaromatics is generated at higher reaction temperatures[29,33,34]. Ni/Z[11.91] exhibits the lowest catalytic activity among all Ni/Z[D] catalysts, selecting no significant products **2a** and **2b** but large amounts of by-products and **2c** (31 %). This specific result will be discussed below.

Based on the catalytic measurements, there are significant variations in product selectivity based on the size of the Ni NPs. However, the information on physicochemical properties is still lacking, such as adsorption affinity, adsorption quantity, and site specificity, on the catalyst surface. TPD with different substrates or probe molecules has been commonly used to provide some quantitative information on the

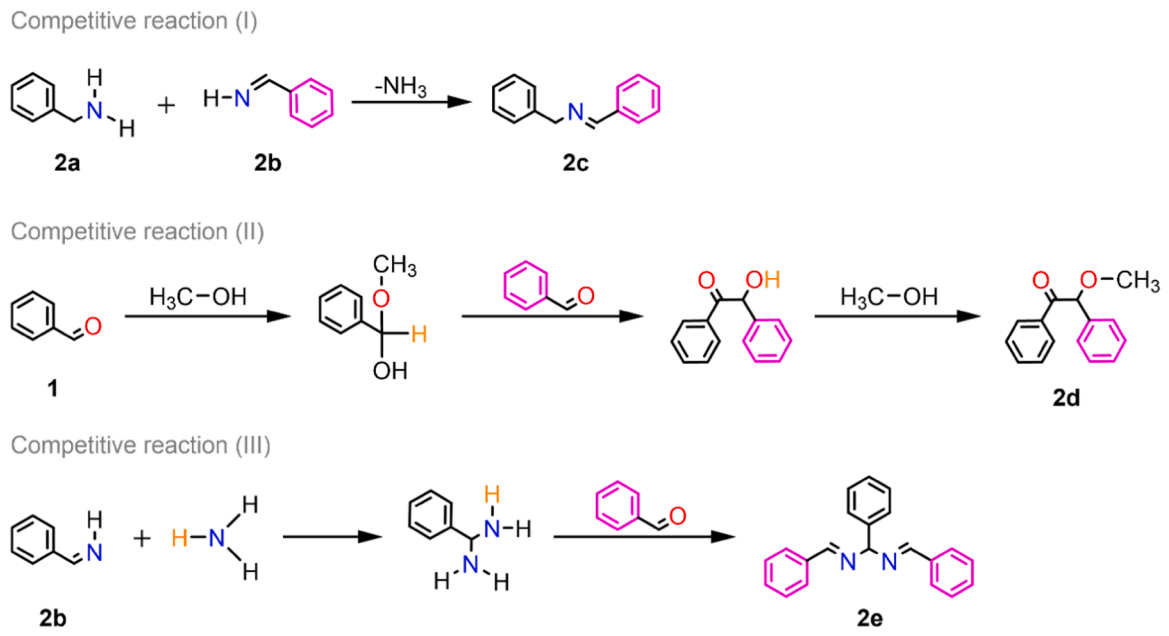

Scheme 3. Competitive reaction pathways in the reductive amination of benzaldehyde.

elucidation of the catalytic performance. Therefore, TPD with ammonia and hydrogen (NH_3-TPD and H_2-TPD) were employed to assess the hydrogenation and amination abilities of the samples in the reduction amination reaction (refer to Figure S7–S8). To minimize interference, such as that from water vapor within the sample, the mass spectroscopy of ammonia ($m/z = 17$) and hydrogen ($m/z = 2$) were directly monitored instead of tracking thermal conductivity detector signals.

The quantitative analyses of the TPD results are presented in Fig. 4**c–d**, revealing distinct changes in the TPD peaks over Ni NPs of different sizes. Fig. 4**c** demonstrates an inverted volcano relationship in desorption temperatures concerning the nanoparticle sizes, with troughs observed in both NH_3-TPD and H_2-TPD over Ni/Z[5.62]. This suggests weaker bindings for ammonia and hydrogen on Ni/Z[5.62], enabling easier desorption from the catalyst surface and potentially facilitating more interactions with the nanoparticles, enhancing their hydrogenation and amination abilities. This increased frequency of interactions should enhance the reaction rate and overall reaction activity. Fig. 4**d** illustrates the desorbed amounts of ammonia and hydrogen by integrating the respective TPD curves. To enable a more direct comparison of the performance differences among the catalysts, the NH_3-TPD and H_2-TPD data were normalized relative to the Ni/Z[5.62] catalyst, and the relative desorption ratios of NH_3 and H_2 were calculated. As shown, the relative H_2 desorption capacity exhibits a volcano-type trend, which correlates well with the catalytic performance for the target product presented in Fig. 4**a**. This further supports the conclusion that the hydrogenation capacity, associated with the formation of Ni NPs, plays a pivotal role in driving the reaction.

Moreover, by comparing the relative NH_3 and H_2 desorption ratios, the balance between hydrogenation and amination capabilities within each catalyst can be assessed. The data indicates that a greater imbalance between these two functionalities correlates with poorer catalytic performance. This trend is especially pronounced under 90 °C (Fig. 4**b**). For Ni/Z[11.91], the amount of hydrogen desorption is significantly lower compared to other catalysts, leading to the lack of catalytic activity even at higher temperatures. The weak hydrogenation ability restricts the formation of the target product while increasing the production of by-products. These findings highlight the importance of functional synergy in catalyst design.

3.3. Nanoparticle size effect

By integrating catalytic data with the physicochemical properties of the catalyst surface, it is observed that the hydrogenation and amination abilities of the catalyst play a complex role in determining reaction selectivity. The comprehensive analysis depicted in Fig. 5, which considers selectivity, nanoparticle size, and reaction pathways, offers an intuitive insight into how size effects influence reductive amination reactions.

Based on catalytic performance, it is inferred that the process of reductive aldehyde amination to primary amines involves a complex reaction network. Due to the high reactivity of aldehydes and the competitive adsorption of imines, at least three side reactions compete with the main reaction: (I) benzylamine and competitively adsorbed imine deamination to form **2c**, (II) aldehyde and alcohol solvent assisted coupling reaction to form **2d**, and (III) unstable imine snatches NH_3 and polymerizes with aldehyde to form **2e**.

As described in Fig. 5, with increasing Ni/Z[D] NPs size (3.72(5) nm – 11.91(7) nm), the catalyst activity characteristics can be categorized into three parts based on hydrogenation and amination capacities. When nanoparticles are small (e.g., Ni/Z[3.72], Ni/Z[3.96]), adsorbed NH_3 and H_2 are blocked on the active sites, which may postpone benzaldehyde with less competitive from generating the intermediate imine, thus reducing the selectivity of benzylamine[35]. As the size grows, the blocking of NH_3 and H_2 slightly decreases, providing more sites for reactant activation, and a shift in competitive reactions from (II) and (III) to (I) was made. Balanced amination and hydrogenation abilities (e.g., Ni/Z[5.62]) result in increased conversion of the substrate to imine. Sufficient active surface hydrides facilitate the formation of intermediates into primary amines, leading to a substantial improvement in selectivity. Further increases in Ni NPs size (e.g., Ni/Z[6.88], Ni/Z[7.98], Ni/Z[11.91]) highlight the weak hydrogenation ability as the main factor affecting reaction selectivity, gradually transitioning competitive reactions from (I) to (III).

Competitive reactions underscore the importance of controlling the key step of the reaction, which is the formation of imine intermediates [36]. The increasing ratio of NH_3 to reactant can enhance imine formation, thereby increasing the proportion of primary amines in the product [37]. However, as NH_3 and amines compete for metal active sites [14,29,38], it is crucial to regulate the catalyst adsorption capacity

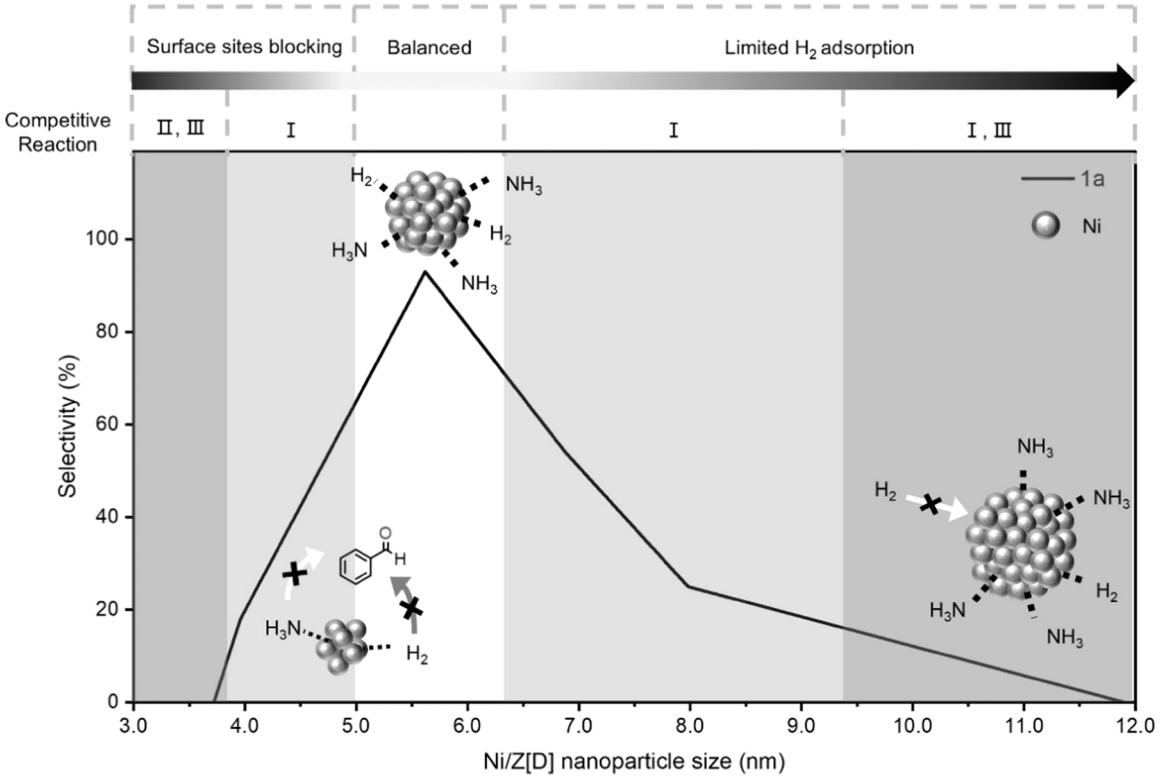

Fig. 5. Reductive amination reaction mechanisms on Ni/Z[D] catalysts with varying nanoparticle sizes.

for NH_3 and H_2 to strike a balance between hydrogenation and amination capacities, which significantly influences reaction selectivity.

To supplement the effect of catalyst structure on the reaction pathway, the distribution of Ni NPs based on the TEM results was analyzed (Figure S9). The spacing between Ni NPs widens with particle size growth, potentially reducing the effective surface area and active sites for hydrogenation and amination, leading to increased polycyclic aromatic hydrocarbons selectivity (-Ph > 3). On metal-supported catalysts, hydrogen dissociation and overflow at the metal site result in a new Brønsted acid site formation next to the Lewis acid center, accelerating the rate of the control step [36]. Dispersion of metal sites may reduce hydrogen dissociation efficiency, slowing imine formation and affecting reaction pathways.

The outcomes of the comprehensive analysis underscore that catalysts of varying particle sizes exhibit different adsorption behaviors for reactants and intermediates, impacting reactant concentrations and ratios on the catalyst surface during reactions, thus influencing catalytic efficiency. This discovery highlights that the particle size of loading metal effectively modulates reactant adsorption strength and capacity. Optimal nanoparticle size facilitates achieving a coordinated 'capacity' ratio, thereby enhancing favorable reaction outcomes. It is essential to note that our primary aim is to gain a profound understanding of the synergistic interactions among proximal active motifs rather than providing an exhaustive account of subsequent reactions.

4. Conclusion

In summary, this study presents a systematic study of Ni NPs with different particle sizes through controlled reduction under hydrogen from uniformly loaded Ni on zeolites. The catalytic activity of the Ni/Z catalyst in reductive amination reactions is found to be strongly dependent on the size of the Ni NPs. Among the catalysts analyzed, the Ni/Z[5.62] sample exhibited the highest catalytic activity with a selectivity of 93 %, owing to an optimal balance between its hydrogenation and amination abilities. In reality, these two capabilities of the catalyst do not align simply or uniformly with the size of the Ni NPs. This may be attributed to the changes in the surface area during aggregation, which can also alter catalytic properties. From Ni/Z[3.72] to Ni/Z[5.62], the loaded metals gradually aggregate on the mesopores or the outer surface of the host matrix, bringing the increased reaction selectivity. As the particle size further increases, the amination and hydrogenation capabilities weaken or become more imbalanced, inducing competitive reactions and lowering the selectivity towards the target product. It should be emphasized that the impact of particle size on catalyst activity is often multifaceted, with the optimization effect varying with target product alterations, necessitating tailored size selection guided by specific target products. These findings contribute to a deeper understanding of how the size of metal particles influences the performance of metal-supported catalysts, thereby facilitating the development of more efficient catalytic systems.

Fundings

This work was financially supported by the National Natural Science Foundation of China (22172136), the Hong Kong Research Grants Council (15305722 and 15301521).

CRediT authorship contribution statement

Lo Benedict: Writing – review & editing, Validation, Supervision, Project administration. **Chen Tianxiang:** Project administration, Methodology. **Wun Ching Kit Tommy:** Methodology, Formal analysis. **Li Yunong:** Writing – original draft, Investigation, Methodology, Formal analysis, Data curation.

Declaration of Competing Interest

The authors declare the following financial interests/personal relationships which may be considered as potential competing interests: Tsz Woon Benedict Lo reports financial support was provided by The

Hong Kong Polytechnic University. Tsz Woon Benedict Lo reports financial support was provided by National Natural Science Foundation of China. Tsz Woon Benedict Lo reports financial support was provided by Research Grants Council (Hong Kong). If there are other authors, they declare that they have no known competing financial interests or personal relationships that could have appeared to influence the work reported in this paper.

Acknowledgment

The author thanks SPring-8 for the provision of valuable synchrotron beamtime for synchrotron XRD, PDF, XAS, and in-situ measurements (2023B1665 and 2023B1666). Finally, we thank the UCEA and the UMF of PolyU for their support in characterization.

Author Contributions

Y.N.L. made major contributions to this work, performed the synthesis, characterization, reactions, data analysis, and wrote the manuscript. C.K.T.W. analyzed the XAS data. T.C. conceived the project, directed the study, and wrote the manuscript. T.W.B.L. conceived the project, directed the study, and wrote the manuscript.

Appendix A. Supporting information

Supplementary data associated with this article can be found in the online version at doi:10.1016/j.mtcata.2025.100100.

References

[1] R. Barra, P. González, Sustainable chemistry challenges from a developing country perspective: education, plastic pollution, and beyond, Curr. Opin. Green. Sust. 9 (2018) 40–44, https://doi.org/10.1016/j.cogsc.2017.12.001.
[2] D. Astruc, F. Lu, J.R. Aranzaes, Nanoparticles as recyclable catalysts: the frontier between homogeneous and heterogeneous catalysis, Angew. Chem. Int. Ed. 44 (2005) 7852–7872, https://doi.org/10.1002/anie.200500766.
[3] R.O. Afolabi, A comprehensive review of nanosystems' multifaceted applications in catalysis, energy, and the environment, J. Mol. Liq. 397 (2024) 124190, https://doi.org/10.1016/j.molliq.2024.124190.
[4] Y. Tian, X. Liu, W. Ma, S. Cheng, L. Zhang, Boosting activity of γ-alumina-supported vanadium catalyst for isobutane non-oxidative dehydrogenation via pure V^{3+}, J. Colloid Interf. Sci. 652 (2023) 508–517, https://doi.org/10.1016/j.jcis.2023.08.098.
[5] G. Silvia, A. Joop, Thomas Peters, Maschmeyer, The reductive amination of aldehydes and ketones and the hydrogenation of nitriles: mechanistic aspects and selectivity control, Adv. Synth. Catal. 344 (2002) 1037–1057, https://doi.org/10.1002/1615-4169(200212)344:10%3C1037::AID-ADSC1037%3E3.0.CO;2-3.
[6] L. Huang, K. Hu, G. Ye, Z. Ye, Highly selective semi-hydrogenation of alkynes with a Pd nanocatalyst modified with sulfide-based solid-phase ligands, Mol. Catal. (2021) 111535, https://doi.org/10.1016/j.mcat.2021.111535.
[7] D. Albani, K. Karajovic, B. Tata, Q. Li, S. Mitchell, N. López, J. Pérez-Ramírez, Ensemble design in nickel phosphide catalysts for alkyne semi-hydrogenation, ChemCatChem 11 (2019) 457–464, https://doi.org/10.1002/cctc.201801430.
[8] N.S. Gould, H. Landfield, B. Dinkelacker, C. Brady, X. Yang, B. Xu, Selectivity control in catalytic reductive amination of furfural to furfurylamine on supported catalysts, ChemCatChem 12 (2020) 2106–2115, https://doi.org/10.1002/cctc.201901662.
[9] D. Chandra, Y. Inoue, M. Sasase, M. Kitano, A. Bhaumik, K. Kamata, H. Hosono, M. Hara, A high performance catalyst of shape-specific ruthenium nanoparticles for production of primary amines by reductive amination of carbonyl compounds, Chem. Sci. 9 (2018) 5949–5956, https://doi.org/10.1039/C8SC01197D.
[10] Y. Wang, S. Furukawa, X. Fu, N. Yan, Organonitrogen chemicals from oxygen-containing feedstock over heterogeneous catalysts, ACS Catal. 10 (2020) 311–335, https://doi.org/10.1021/acscatal.9b03744.
[11] X. Jv, S. Sun, Q. Zhang, M. Du, L. Wang, B. Wang, Efficient and mild reductive amination of carbonyl compounds catalyzed by dual-function palladium nanoparticles, ACS Sustain. Chem. Eng. 8 (2020) 1618–1626, https://doi.org/10.1021/acssuschemeng.9b06464.
[12] J.I. Ramsden, R.S. Heath, S.R. Derrington, S.L. Montgomery, J. Mangas-Sanchez, K. R. Mulholland, N.J. Turner, Biocatalytic *N* -alkylation of amines using either primary alcohols or carboxylic acids via reductive aminase cascades, J. Am. Chem. Soc. 141 (2019) 1201–1206, https://doi.org/10.1021/jacs.8b11561.
[13] A. Ruffoni, F. Juliá, T.D. Svejstrup, A.J. McMillan, J.J. Douglas, D. Leonori, Practical and regioselective amination of arenes using alkyl amines, Nat. Chem. 11 (2019) 426–433, https://doi.org/10.1038/s41557-019-0254-5.
[14] D. Luo, Y. He, X. Yu, F. Wang, J. Zhao, W. Zheng, H. Jiao, Y. Yang, Y. Li, X. Wen, Intrinsic Mechanism of Active Metal Dependent Primary Amine Selectivity in the Reductive Amination of Carbonyl Compounds, J. Catal. 395 (2021) 293–301, https://doi.org/10.1016/j.jcat.2021.01.016.
[15] J. Gallardo-Donaire, M. Ernst, O. Trapp, T. Schaub, Direct Synthesis of Primary Amines *via* Ruthenium-Catalysed Amination of Ketones with Ammonia and Hydrogen, Adv. Synth. Catal. 358 (2016) 358–363, https://doi.org/10.1002/adsc.201500968.
[16] J.J. Martínez, E. Nope, H. Rojas, M.H. Brijaldo, F. Passos, G. Romanelli, Reductive Amination of Furfural over Me/SiO_2-SO_3H (Me: Pt, Ir, Au) Catalysts, J. Mol. Catal. A-Chem. 392 (2014) 235–240, https://doi.org/10.1016/j.molcata.2014.05.014.
[17] K. Zhou, H. Liu, H. Shu, S. Xiao, D. Guo, Y. Liu, Z. Wei, X. Li, A Comprehensive Study on the Reductive Amination of 5-Hydroxymethylfurfural into 2,5-Bisaminomethylfuran over Raney Ni Through DFT Calculations, ChemCatChem 11 (2019) 2649–2656, https://doi.org/10.1002/cctc.201900304.
[18] K. Murugesan, M. Beller, R.V. Jagadeesh, Reusable Nickel Nanoparticles-Catalyzed Reductive Amination for Selective Synthesis of Primary Amines, Angew. Chem. Int. Ed. 131 (2019) 5118–5122, https://doi.org/10.1002/ange.201812100.
[19] E. Kolobova, P. Mäki-Arvela, A. Pestryakov, E. Pakrieva, L. Pascual, A. Smeds, J. Rahkila, T. Sandberg, J. Peltonen, D.Yu Murzin, Reductive Amination of Ketones with Benzylamine Over Gold Supported on Different Oxides, Catal. Lett. 149 (2019) 3432–3446, https://doi.org/10.1007/s10562-019-02917-1.
[20] J.H. Cho, S.H. An, T.-S. Chang, C.-H. Shin, Effect of an Alumina Phase on the Reductive Amination of 2-Propanol to Monoisopropylamine Over Ni/Al_2O_3, Catal. Lett. 146 (2016) 811–819, https://doi.org/10.1007/s10562-016-1695-8.
[21] Z. Pan, Q. Zhang, W. Wang, L. Wang, G.-H. Wang, Size-Tunable Carbon-Doped Ni Nanoparticles for Switchable Reductive Amination of Biomass-Derived Carbonyl Compounds to Primary Amines and Secondary Imines, ACS Sustain. Chem. Eng. 10 (2022) 3777–3786, https://doi.org/10.1021/acssuschemeng.2c00800.
[22] H. Wu, Q. Wang, Y. Zhao, Z. Gao, Y. Lin, L. Zheng, D. Li, J. Feng, Coupling Cross-Dimensional Ru_1-Ru_n Sites in Confined Nanoislands to Overcome the Limitation of Coadsorption and Diffusion in Tandem Reactions, ACS Catal. 14 (2024) 1584–1594, https://doi.org/10.1021/acscatal.3c05112.
[23] G. Fu, Y. Li, Z. Hou, S. Wang, S. Jiang, T. Chen, T.W. Benedict Lo, X. Chen, Diatomic Cobalt–catalyzed Cyclization of O-aminobenzyl Alcohol with Amidine for the Synthesis of Quinazolines, J. Catal. 442 (2025) 115889, https://doi.org/10.1016/j.jcat.2024.115889.
[24] N. Miletić, U. Izquierdo, I. Obregón, K. Bizkarra, I. Agirrezabal-Telleria, L.V. Bario, P.L. Arias, Oxidative steam reforming of methane over nickel catalysts supported on $Al_2O_3CeO_2$-La_2O_3, Catal. Sci. Technol. 5 (2015) 1704–1715, https://doi.org/10.1039/C4CY01438C.
[25] T.A. Le, T.W. Kim, S.H. Lee, E.D. Park, CO and CO_2 Methanation over Ni Catalysts Supported on Alumina with Different Crystalline Phases, Korean J. Chem. Eng. 34 (2017) 3085–3091, https://doi.org/10.1007/s11814-017-0257-0.
[26] Z. Zhou, X. Wang, R. Yu, R. Jiang, Y. Gao, X. Chen, H. Hou, Synthesis of b-axis oriented ZSM-5 zeolite by mechanochemical-assisted quasi-solvent-free method and its MTO catalytic performance, Adv. Powder Technol. 34 (2023) 103930, https://doi.org/10.1016/j.apt.2022.103930.
[27] Y. Li, G. Zhu, Y. Wang, Y. Chai, C. Liu, S. He, In situ construction of an immobilized b-oriented titanium silicalite spherical molecular sieve membrane, Appl. Surf. Sci. 563 (2021) 150275, https://doi.org/10.1016/j.apsusc.2021.150275.
[28] B.T.W. Lo, Y.-K. Peng, S.-C.E. Tsang, Surface Coordination Chemistry of Nanomaterials and Catalysis, in: C. Edwin, P. Gerard, Q. Lawrence (Eds.), Comprehensive Coordination Chemistry III: From Biology to Nanotechnology, 3rd ed, Elsevier, 2021, pp. 204–227, https://doi.org/10.1016/B978-0-08-102688-5.00017-9.
[29] J. Krupka, L. Dluhoš, L. Mrózek, Evaluation of Benzylamine Production via Reductive Amination of Benzaldehyde in a Slurry Reactor, Chem. Eng. Technol. 40 (2017) 870–877, https://doi.org/10.1002/ceat.201600538.
[30] T. Irrgang, R. Kempe, Transition-Metal-Catalyzed Reductive Amination Employing Hydrogen, Chem. Rev. 120 (2020) 9583–9674, https://doi.org/10.1021/acs.chemrev.0c00248.
[31] J.-W. Kou, S.-Y. Cheng, J.-W. Wang, X.-M. Xie, Synthesis and Characterization of Cu/Cr Hydrotalcite-like Compounds and their Highly Efficient Application in Catalytic Synthesis of Benzoin Methyl Ether, Chem. Eng. J. 323 (2017) 565–571, https://doi.org/10.1016/j.cej.2017.04.125.
[32] Q. Lu, J. Sun, X.-Z. Wei, Q. Zhang, X. Zhang, L. Chen, J. Liu, Y. Chen, L. Ma, Switchable Reductive Amination of Aldehydes over Metal-encapsulated S-1 Zeolites with Tunable Acid-base Properties, Appl. Catal. A-Gen. 678 (2024) 119653, https://doi.org/10.1016/j.apcata.2024.119653.
[33] N.E. Sánchez, A. Callejas, Á. Millera, R. Bilbao, M.U. Alzueta, Polycyclic Aromatic Hydrocarbon (PAH) and Soot Formation in the Pyrolysis of Acetylene and Ethylene: Effect of the Reaction Temperature, Energ. Fuel 26 (2012) 4823–4829, https://doi.org/10.1021/ef300749q.
[34] K. Arnesen, T.A. Aarhaug, K.E. Einarsrud, G.M. Tranell, Influence of Atmosphere and Temperature on Polycyclic Aromatic Hydrocarbon Emissions from Green Anode Paste Baking, ACS Omega 8 (2023) 18116–18121, https://doi.org/10.1021/acsomega.3c01411.
[35] F. Santoro, R. Psaro, N. Ravasio, F. Zaccheria, Reductive Amination of Ketones or Amination of Alcohols over Heterogeneous Cu Catalysts: Matching the Catalyst Support with the N-Alkylating Agent, ChemCatChem 4 (2012) 1249–1254, https://doi.org/10.1002/cctc.201200213.
[36] J.D. Vidal, M.J. Climent, P. Concepcion, A. Corma, S. Iborra, M.J. Sabater, Chemicals from Biomass: Chemoselective Reductive Amination of Ethyl Levulinate

with Amines, ACS Catal. 5 (2015) 5812–5821, https://doi.org/10.1021/acscatal.5b01113.
[37] C.F. Winans, Hydrogenation of Aldehydes in the Presence of Ammonia, J. Am. Chem. Soc. 61 (1939) 3566–3567, https://doi.org/10.1021/ja01267a102.
[38] T.A. Gokhale, A.B. Raut, B.M. Bhanage, Comparative Account of Catalytic Activity of Ru- and Ni-based Nanocomposites towards Reductive Amination of Biomass Derived Molecules, Mol. Catal. 510 (2021) 111667, https://doi.org/10.1016/j.mcat.2021.111667.